ACS OMEGA

Open Access

This article is licensed under CC-BY-NC-ND 4.0

http://pubs.acs.org/journal/acsodf

Article

CO Diffusion Study and Spatial and Temporal Variation Modeling during the Construction Period of the Plateau Railroad Tunnel

Jie Liu, Huyun Zhao, Wanqing Wang,* Haowen Zhou, Feng Lu, Liting Wan, Xuehua Luo, and Liangyun Teng

Cite This: *ACS Omega* 2023, 8, 42565−42575

Read Online

ACCESS | Metrics & More | Article Recommendations

ABSTRACT: In order to investigate the diffusion law of CO gas in the vicinity of the tunnel boring face of the plateau long tunnel, to improve the efficiency of tunnel smoke exhaust, and to derive the spatial-temporal variation model of CO concentration for predicting the concentration of CO at different times and in different cross sections under specific environments, a CO diffusion model of a tunnel in Yunnan was established by using Ansys Fluent Fluid Simulation Software, and the CO transport characteristics under different conditions were simulated by taking the ventilation time, wind speed, and location of the air ducts as the influencing factors. The results show that the wind flows from the mouth of the wind pipe after the wind speed decreases, the diffusion area increases and arrives at the face of the direction of the rebound in the jet stream of new wind, and the return wind under the joint action of the vortex produced obviously, to reach the wind pipe mouth after the tunnel wind flow field, basically tends to stabilize. When the wind pipe mouth was arranged in the arch waist, 20 m away from the boring face, the inlet wind speed was 9 m/s and the ventilation time was 30 min; the CO concentration in the tunnel was reduced to below the maximum allowable concentration value. Moreover, the concentration of CO in the tunnel at the moment of 15 min of ventilation has a nonlinear positive correlation with the change of distance L from the boring face, while at the cross section of the air outlet of the wind pipe L = 20 m, the ventilation time is from 1 to 30 min and the concentration of CO at the cross section has a nonlinear decreasing trend with the ventilation time, which can be deduced according to the different space−time change models.

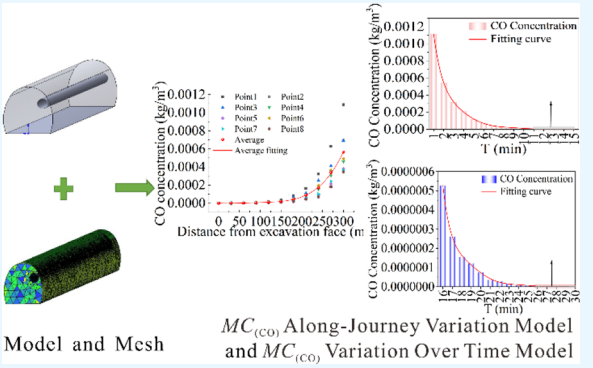

1. INTRODUCTION

At present, the drill and blast method has often been used for tunnel excavation; during the tunnel blasting construction process, a large amount of dust, CO, and other hazardous substances is generated, which poses great threat to the health of the workers due to the long-term exposure of these hazardous substances in the construction environment. Workers are susceptible to occupational pneumoconiosis and other respiratory diseases, which account for more than 90% of the legally recognized occupational diseases in China and are more severe at high altitudes.[1−4] Because the increasing altitude, low temperature, low oxygen, low pressure, and other factors will inevitably bring new challenges to the construction of high-altitude tunnels, the low-oxygen environment of the plateau explosives is not sufficiently combusted and will produce more toxic and harmful gases than the plain explosives, in which CO easily combines with human hemoglobin, so as to asphyxiate or even cause death; thus, exploring the characteristics of the diffusion of toxic and harmful gases in the high-altitude tunnels and accurately predicting the change of the concentration of CO in the tunnels are necessary.[5−7]

In terms of CO transport law in tunnels, Harris and other scholars,[8−12] through on-site monitoring of CO concentration data in tunnels, analyzed the pattern of change of the monitoring data and derived the distribution of CO in tunnels over time; Torno and other scholars,[13−16] using the hydrodynamics software to establish a reasonable roadway tunnel model, defined the smoke that is blown out of the gun after the blasting time, analyzed the distribution of gun smoke under different blasting conditions, and predicted when workers could enter the workplace after blasting; Vorontsov and others[17−19] established a model of gun smoke diffusion in the roadway, concluded that the gun smoke diffusion law was significantly affected by the wind flow, and derived the calculation formula of the CO dispersion coefficient of the tunneling roadway; Zhou and

Received: July 21, 2023
Revised: August 21, 2023
Accepted: October 16, 2023
Published: November 2, 2023

© 2023 The Authors. Published by American Chemical Society

others[20−23] analyzed the basic theory of mine ventilation and made a systematic research on the aspects of the mine ventilation system and the local ventilation of the mine and quarry; and so on. In addition, in-depth research has also been conducted on the ventilation design of the quarry, wind flow, and the transportation law of gas; Zhong'an and others[24−27] numerically simulated the soot flow after blasting in the tunnel and gave an optimal ventilation scheme for the actual engineering situation, which provided a reference basis for the numerical simulation of soot ventilation in the tunnel. Lijun and others[28−31] proposed a formula for calculating the discharge of gun smoke in underground engineering, discussed the shortcomings of the existing ventilation airflow calculation method for tunnel blasting and digging, and verified it with the field measurement data; Cui and others[32−35] studied the transportation and distribution law of blasting smoke in tunnels and mines under natural ventilation. In coal mine ventilation, Juganda and others[36,37] provided a theoretical basis of CFD and, using numerical simulation, analyzed and summarized that fluid dynamics can be used in simulation to solve the hazards of coal mine gas explosion, fire, dust explosion, high heat, and humidity, as well as to identify poor-ventilation areas in which methane air tends to accumulate, areas where methane air tends to accumulate, and to design a reasonable ventilation method to solve the hazards to the greatest extent.

Although the experts and scholars mentioned above have done a lot of research, in general, the theoretical models they have come up with are biased toward the regional level and may be less applicable. In addition, most of their research results are based on the background of low-altitude mines and tunnels and their theories are not sufficiently applicable to high-altitude tunnels. In high-altitude tunnels, the atmospheric environment was quite different from that of the plains, with greater variations in atmospheric pressure, temperature, and humidity and with lower oxygen levels. Normally, the accuracy of data collected in the field is higher, but due to various constraints, the collection work may be more difficult. While the data obtained from indoor experiments often differ greatly from reality, numerical simulations using software have the advantage of being more convenient and accurate. Therefore, the purpose of this paper is to predict the change of the CO concentration in tunnels by fitting a mathematical model and derive the safe re-entry time, which provides a preliminary reference for indoor experiments and on-site validation.

The purpose of this study was to simulate the CO gas transport and concentration change after blast ventilation in the tunnel boring face based on the low pressure, low oxygen, and low temperature of the plateau environment where the tunnel was located, to establish a prediction model to study the CO concentration change in the tunnel, and to verify the accuracy of the simulation results through the field measurement data and then use the results of numerical simulation to establish a predictive CO mass concentration of the $MC_{(CO)}$ spatial-temporal variation model, compared with the previous derivation of the ventilation air volume formula, ventilation program optimization and improvement methods, and underground engineering smoke discharge formula; the model obtained in this paper can be used to calculate the specific conditions of the tunnel of different cross sections and different time changes in the concentration of CO for the use of the drilling and blasting method of construction of tunnels. Theoretical support is provided as well for the ventilation of tunnels constructed by the drilling and blasting method.

2. MATERIALS AND METHODS

2.1. Geometric Model and Meshing. This paper takes a tunnel in Yunnan as the research background; according to the on-site investigation and measurement, the altitude of the tunnel location is about 1650 m, the atmospheric pressure is about 82.5% of the atmospheric pressure at sea level, and the oxygen content in the air is lower about 18%; the whole tunnel belongs to the subtropical monsoon climate in the mountainous area, and the average annual temperature is 25.2 °C. The tunnel is also known as the world's most "poisonous gas" tunnel because of the many types of toxic and harmful gases in it, the concentration is high, and the degree of harm is great, which contains eight kinds of toxic and harmful gases, such as H_2S, NO_x, and CO. The tunnel starts and ends at DK114 + 497−DK125 + 113, with a total length of 10,616 m. The maximum depth of the tunnel is 867 m, and the minimum depth is 568 m; the tunnel section is a single elliptical arch with a clear height of 7.1 m and a width of 6.3 m, with a total section area of 41.5 m^2. The site adopts a press-in type wind pipe, which is located at the waist of the arch at a height of 4.6 m above the ground in the tunnel, the outlet of the wind pipe is 20 m away from the face of the palm, and the diameter of the pipe is 1.6 m, with the wind speed of 9 m/s. The geometric model of the tunnel with a length of 300 m was drawn using the modeling software SOLIDWORKS, and after determining the geometric model, a topological check was carried out; all the lines were red solid lines, indicating that the model was a nonvulnerable entity. ICEM CFD was used for meshing; the grid type of the mesh was nonstructural tetrahedral, no. 36420, its quality was higher than 0.3, and its minimum internal angle was greater than 18°, to meet the requirements of the subsequent calculations. The geometric model of the tunnel map and the mesh division of the specific situation are shown in Figure 1.

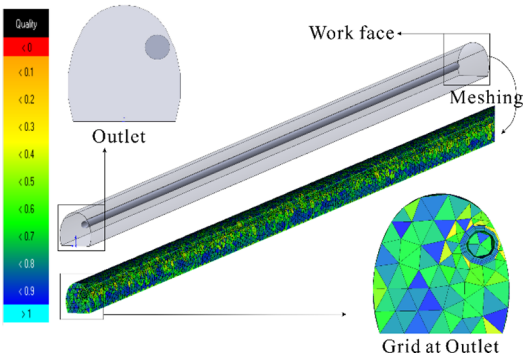

Figure 1. Geometric model and meshing.

In the simulation, the calculation speed and accuracy of the calculation results are closely related to the quality of the mesh delineation; therefore, mesh independence check is a very important part before the numerical simulation. The ICEM CFD is used to divide the mesh and encrypt it in the turbulent region of the flow field, and three different numbers of meshes are obtained after encryption, i.e., mesh 1—29650, mesh 2—36420, and mesh 3—43890. For the height of the breathing zone taking the centerline consistent with the direction along the tunnel exit and observing the wind speed size, the results are shown in Figure 2. The sparseness of the tunnel grid division is different, but the wind speed size and the trend of change under the different grids are relatively close to each other, and the relative error is less than 10%. Therefore, according to the

https://doi.org/10.1021/acsomega.3c05280
ACS Omega 2023, 8, 42565−42575

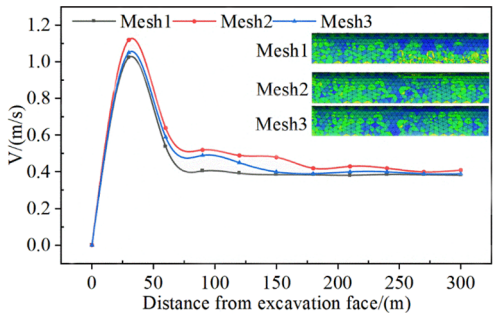

Figure 2. Variation of wind speed along different meshes.

requirements of the performance of the computer and the accuracy of the calculation, mesh 2 was selected for numerical computation;[38] the computational time step was 0.1 s, the total number of iterative steps was 18,000, and the maximum iterative time steps were 20. In addition, the SIMPLE algorithm was used to calculate the transportation of CO in the tunnel within 30 min.

2.2. Mathematical Model. Tunnel construction blasting produces a large amount of CO gas; CO is diluted by the air wrapped, and the process of discharging it out of the tunnel is a single-phase multicomponent diffusion problem without chemical reaction, with a Reynolds number greater than 8000 for turbulence flow state. Therefore, a set of equations were applied for the control of CO transport to take into account the law of conservation of mass, the law of conservation of momentum, and the law of conservation of energy, which were also considered in the equation of component conservation as well as the equation of turbulence and kinetic energy.[38]

1. Continuity equation:

This equation indicates that the increase in fluid microelement per unit time is equal to the net mass flowing into the microelement.

$$\frac{\partial \rho}{\partial t} + \frac{\partial}{\partial x_i}(\rho u_i) = 0 \tag{1}$$

2. Momentum conservation equation:

This equation represents the rate of change of the momentum of a fluid microelement with respect to time equal to the sum of the various external forces on the fluid microelement.

$$\frac{\partial}{\partial t}(\rho u_i) + \frac{\partial}{\partial x_j}(\rho u_i u_j) = -\frac{\partial p}{\partial x_i} + \frac{\partial \tau_{ij}}{\partial x_j} + \rho g_i + F_i \tag{2}$$

3. Energy conservation equation:

$$\frac{\partial(\rho T)}{\partial t} + \frac{\partial(\rho u_j T)}{\partial x_j} = \frac{\partial}{\partial x_j}\left[\frac{\mu_t}{\sigma T}\frac{\partial T}{\partial x_j}\right] + \frac{C_{pv} - C_{pa}}{C_p}\left[\left(\frac{\mu_t}{\sigma T}\right)\frac{\partial w}{\partial x_j}\right]\frac{\partial T}{\partial x_j} \tag{3}$$

In eqs 1−3, the meaning of each parameter is as follows: t is time, s; u_i is the velocity of the fluid in direction i, m/s; x_i is the coordinate in direction i, m; x_j is the coordinate in direction i, m; ρ is the gas density, kg/m^3; τ_{ij} is the stress tensor; g_i is the gravitational acceleration in direction i, m/s^2; F_i is the fluid resistance, N; T is the temperature, K; μ_i is the turbulent viscosity coefficient, Pa·s; μ_t is the turbulent viscosity of the fluid, kg/(m·s); C_p is the specific heat of mixture fluid at constant pressure, J/(kg·K); C_{pv} is the constant pressure-specific heat of the leaking substance, J/(kg·K); and C_{pa} is the constant pressure-specific heat of air, J/(kg·K).

4. Group conservation equation:

$$\frac{\partial(\rho Y_i)}{\partial t} + \nabla \times (\rho v Y_i) = -\nabla \times J_i + R_i + S_i \tag{4}$$

5. The standard $k-\varepsilon$ turbulent double equations are as follows:

$$\frac{\partial}{\partial t}(\rho k) + \frac{\partial}{\partial x_i}(\rho k u_i) = \frac{\partial}{\partial x_j}\left[(\mu + \frac{\mu_i}{\sigma_k})\frac{\partial k}{\partial x_j}\right] + G_k + G_b - \rho\varepsilon - Y_M + S_k \tag{5}$$

$$\frac{\partial}{\partial t}(\rho\varepsilon) + \frac{\partial}{\partial x_i}(\rho\varepsilon u_i) = \frac{\partial}{\partial x_j}\left[(\mu + \frac{\mu_t}{\sigma_\varepsilon})\frac{\partial \varepsilon}{\partial x_j}\right] + C_{1\varepsilon}\frac{\varepsilon}{k}(G_k + C_{3_\varepsilon}G_b) - C_{2\varepsilon}\rho\frac{\varepsilon^2}{k} + S_\varepsilon \tag{6}$$

In eqs 4−6, the meaning of each parameter is as follows: R_i is the net production rate of chemical reaction product i; S_i is the extra production rate; Y_i is the mass fraction of component i; and J_i is the diffusion flux of component i. G_k is the term for the generation of turbulent kinetic energy k due to the velocity gradient; G_b is the term for the buoyancy-induced generation of turbulent kinetic energy k; Y_M is the kinetic energy generation term due to the compressibility of the fluid; S_k is the turbulent energy term; μ is the laminar viscosity factor, Pa·s; S_ε is the turbulent kinetic energy dissipation rate source term; and $C_{1\varepsilon}$, $C_{2\varepsilon}$, C_μ, σ_k, and σ_ε are constants, equal to 1.44, 1.92, 0.09, 1.3, and 1.0, respectively.

2.3. Basic Assumptions. Due to the actual working conditions and simulation of certain differences, the modeling is not possible to completely restore the site, so the simulation needs to make certain assumptions about the project. According to the field measurement and calculation conditions, under the premise of acceptable error and little impact on the accuracy of the results, the following assumptions are made for the diffusion of smoke generated after blasting:

1. CO and other substances in the tunnel will react accordingly, but because the content is very small and the final results of the impact are negligible, it is assumed that the nature of CO is stable and will not react with other substances in the tunnel.
2. CO and air are incompressible and ideal viscous fluids.
3. Although there are changes in the tunnel environmental and climatic conditions such as temperature, humidity, atmospheric pressure, and oxygen content, because of the small impact, it is assumed that the climate conditions remain unchanged.
4. The toxic and harmful gases produced by blasting are CO, CO_2, NO, NO_2, H_2S, etc., but the content of several other

https://doi.org/10.1021/acsomega.3c05280
ACS Omega 2023, 8, 42565−42575

gases aside from CO is relatively small, so this paper focuses on CO as the object of study.

5. The CO content of the fresh air output from the ventilator is zero.

2.4. Parameter Settings. After the meshing is completed, it is imported into Ansys Fluent software for numerical calculation. Before the calculation, the following boundary conditions and model parameters are set for the model, as shown in Table 1 and Table 2.

Table 1. Boundary Condition Setting

boundary condition	setting	boundary condition	setting
inlet boundary	velocity inlet	outlet boundary	outflow
wall	standard wall function	time	transient
solver	pressure-based	wall boundary	no slip

Table 2. Model Parameter Setting

calculation model	setting	calculation model	setting
inlet velocity	9 m/s	gauge pressure	−18,319 Pa
pressure	83,006 Pa	oxygen content	18%
hydraulic diameter	1.2 m	air duct diameter	1.6
air density	1.0419 kg/m^3	species transport	on
turbulent intensity	3.14%	energy	on
temperature	25 °C	viscous	standard $k-\varepsilon$
initial CO concentration	0.0025 kg/m^3		

The formula of the hydraulic diameter d_H is as follows:

$$d_H = \frac{4A}{S} \tag{7}$$

In eq 7, d_H is the hydraulic diameter, m; A is the cross-sectional area of the flow, m^2; and S is the cross-sectional perimeter of the flow, m.

The formula of turbulent intensity I is as follows:

$$I = \frac{u'}{\overline{u}} = 0.16(Re_{d_H})^{-\frac{1}{8}} \tag{8}$$

In eq 8, I is the turbulent intensity, u' is the turbulent pulsation velocity, m/s; and $\overline{u}$ is the average flow velocity, m/s.

The calculation formula of the initial CO concentration is as follows:

$$C = \frac{m_G b}{L_{gas} A} \tag{9}$$

In eq 9, C is the initial CO concentration, kg/m^3; m_G is the amount of explosive used once during excavation, kg; b is the volume of noxious gas produced after blasting of 1 kg of explosive, m^3; and L_{gas} is the harmful gas migration distance, m.

3. RESULTS AND DISCUSSION

3.1. Wind Flow Law Analysis. By summarizing the previous research, it is known that the toxic and hazardous gases in the construction tunnel are mainly affected by the tunnel wind flow field and the stability of the wind flow field is related to the flow of gases in the tunnel; therefore, it is necessary to analyze the structure of the wind flow field in the tunnel. After a period of ventilation, the wind flow field gradually tends to stabilize. After the numerical simulation and postprocessing of ventilation, the wind flow trace map near the boring face and the wind speed cloud map at different heights were plotted, as shown in Figure 3 and Figure 4.

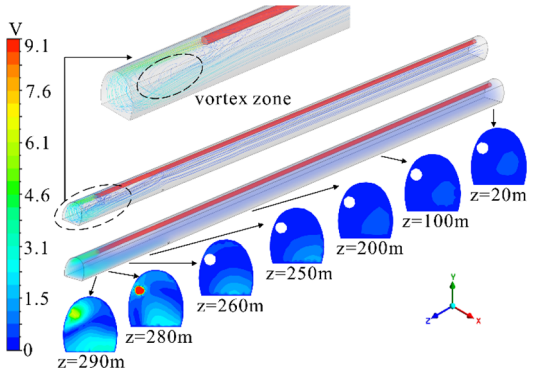

Figure 3. Air flow streamline and velocity field distribution.

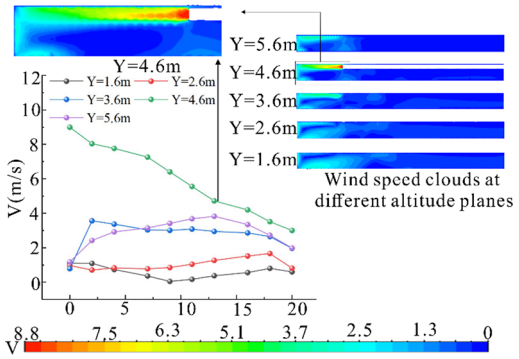

Figure 4. Different-height-velocity cloud diagram.

From Figure 3, it can be seen that the fresh wind flows from the mouth of the wind pipe into the tunnel, and along the tunnel wall, it flows to the face of the tunnel to form a jet zone; the fresh wind flow in the jet zone leaves the wind pipe and continues to flow forward to reach the face of the tunnel. The wind speed decreases to 0.8−3.5 m/s after contacting with the boring face, and the flow direction rebounds. With the diffusion of the wind flow, the diffusion section increases and the wind speed decreases and part of the gas in contact with the tunnel wall continues to flow along the wall to the tunnel opening and diffuses to the middle section of the tunnel, thus forming the wind flow backflow area. The other part of the gas in the jet area of fresh gas and the reflux area under the joint action of the roll suction to form a vortex area with an average wind speed of about 0.8 m/s. Wind speed changes are not obvious, but the gas is in the state of repeated cyclotron, which is likely to lead to CO gas aggregation in this area, the greater the impact on the discharge of CO gas.

From the velocity cloud diagram of the tunnel plane at different heights in Figure 3, the velocity of wind flow at each height plane can be seen; comparing the velocity cloud diagram at each height, the fresh air flow from the wind pipe shoots along the jet area to reach the boring face and then rebound in the vicinity of the boring face to form a vortex area. From the velocity map at the height of Y = 4.6 m, it can be seen that the airflow conforms to the characteristics of the wall-constrained jet; i.e., the fresh air moves forward along the wall on the side of the mouth of the wind pipe, and the section of the jet is

https://doi.org/10.1021/acsomega.3c05280
ACS Omega 2023, 8, 42565−42575

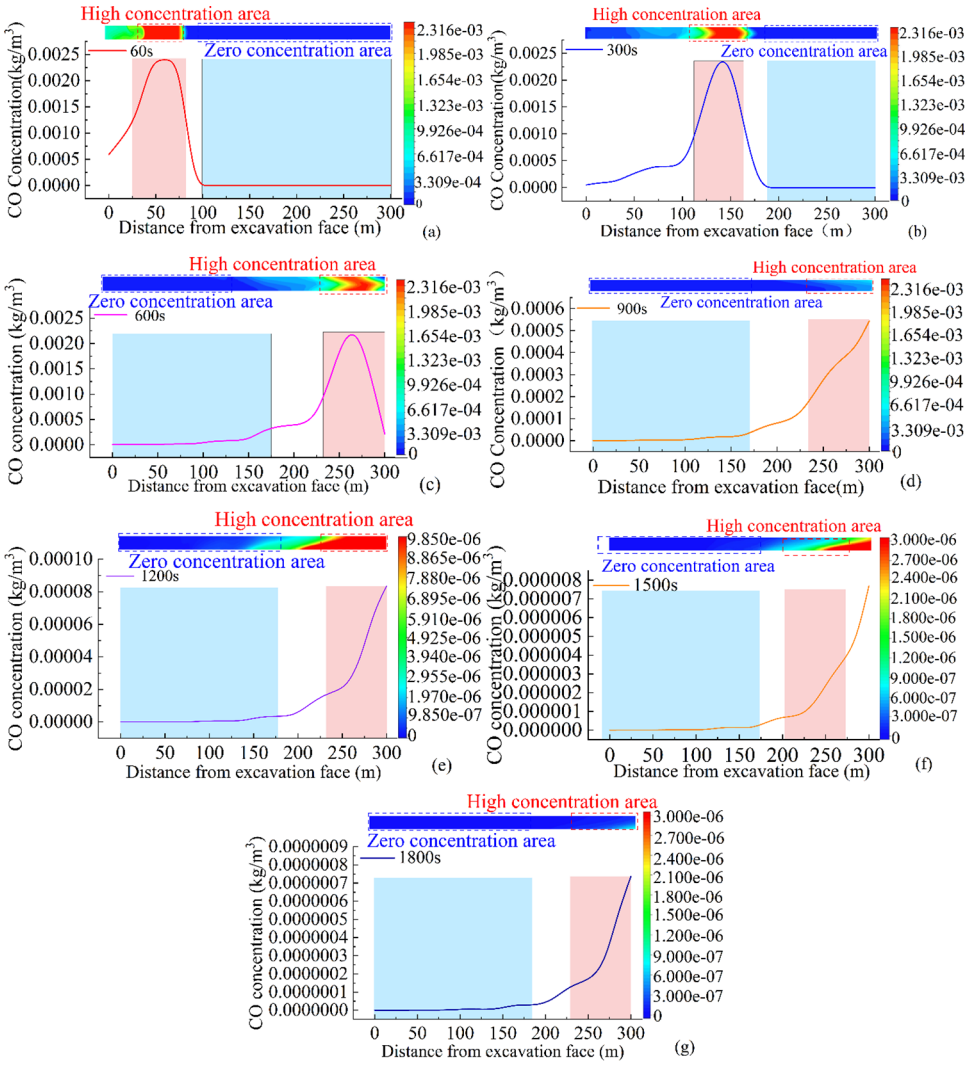

Figure 5. Variation of CO concentration with time (a−g: The changes of CO concentration from 60 to 1800 s).

constantly increasing while the velocity is constantly decreasing. When the fresh air arrives at the digging surface, it will return due to the obstruction of the digging surface; the returning air interacts with the fresh air coming out from the wind pipe, and the air flow is disordered, thus generating the vortex phenomenon.

3.2. Effect of Different Ventilation Durations on the Distribution of CO. In order to study the rule of change of the CO concentration with time in the tunnel, the pressure-entry air blower is set at 20 m from the boring face and the wind speed is 9 m/s. The distribution of CO in the human respiratory zone Y = 1.6 m plane in the tunnel is analyzed by taking the moments of t = 60 s, 300 s, 600 s, 900 s, 1200 s, 1500, and 1800 s in the time period of ventilation for 30 min, respectively.[39] The variation of the CO with time is shown in Figure 5

As can be seen from Figure 5a, after blasting in the tunnel, due to the existence of the throwing zone, the CO gas mainly gathers in the position of about 60 m from the face of the tunnel to form a high-concentration zone in the 60 s of ventilation; at this time, the highest concentration of CO gas in this area is about 2450 mg/m^3, which is in line with the actual calculated value, and the concentration of CO gas in the vicinity of the face of the tunnel is reduced from 2450 to about 549 mg/m^3. With the continuous supply of the wind turbine, the CO gas is sucked by the fresh air flow to move to the middle of the tunnel in the shape of air mass and the CO concentration in the front of the air mass shows the phenomenon of high in the middle and low in the two ends, while in the back of the air mass, the opposite is true, which is because the gas is affected by the confined jet characteristics of the wall, resulting in slower diffusion of CO near the wall surface. After 1200 s of ventilation, the CO gas in the tunnel is discharged to the tail of the tunnel and the peak value of the high-concentration band is changed to 0.00083 kg/m^3; at this time, the CO concentration in the area of 150 m from the boring face has already met the provisions of the *Railway Tunnel Design Specification (TB10003-2016)*, hereinafter referred to as the *Design Specification*, and the maximum permissible concentration of CO is 30 mg/m^3. The maximum allowable concentration of CO is 30 mg/m^3. From Figure 5f, it can be seen that CO is basically discharged when the tunnel is ventilated for 1500 s and only a small amount of CO remains in the tail of the tunnel, with the maximum concentration of 8 mg/m^3, and it is only necessary to continuously ventilate the tunnel for 1800 s to discharge all the CO gases out of the tunnel.

3.3. Effect of Different Inlet Wind Speeds on the Distribution of CO. In order to study the effect of different wind speeds at the entrance on the CO transport pattern in the construction tunnel, a wind pipe is set at 20 m from the boring

https://doi.org/10.1021/acsomega.3c05280
ACS Omega 2023, 8, 42565−42575

face and the wind speeds are set to 5.8, 7.2, and 9 m/s. According to the relevant provisions of the *Design Specification*, the nongas blasting work area is allowed to enter the boring face after 15 min under the condition of checking without error. Therefore, the diffusion of CO under different wind speeds at the time of ventilation time t = 60 s, 180, 300, 420, 540, 660, 780, and 900 s is simulated, and the results are shown in Figures 6, 7, and 8.

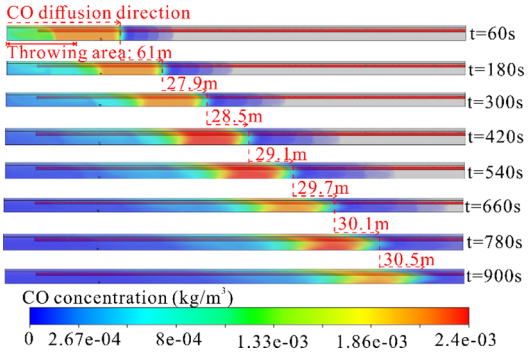

Figure 6. Diffusion of CO at wind speed of 5.8 m/s.

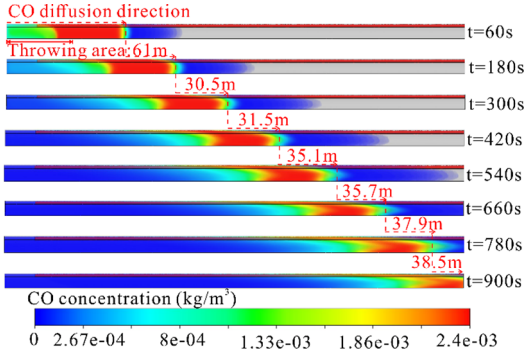

Figure 7. Diffusion of CO at wind speed of 7.2 m/s.

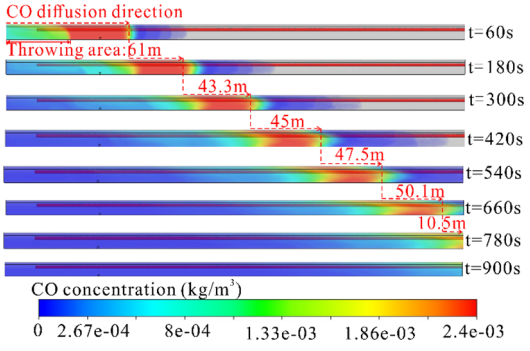

Figure 8. Diffusion of CO at a wind speed of 9 m/s.

3.4. Effect of Different Outlet Positions of the Air Duct on the Distribution of CO. In order to study the influence of different duct locations on the CO distribution in the tunnel, different locations of ducts were set up in the tunnel for numerical simulation at the arch waist, arch top, and arch foot. When the wind speed is 9 m/s, t = 60 s and t = 660 s are taken to compare and analyze the CO concentration maps in the Y = 1.6 m-height plane under these three kinds of air ducts, as shown in Figures 9, 10, and 11.

From Figures 9, 10, and 11, it can be seen that the distribution of CO in the tunnel is more or less the same no matter what kind

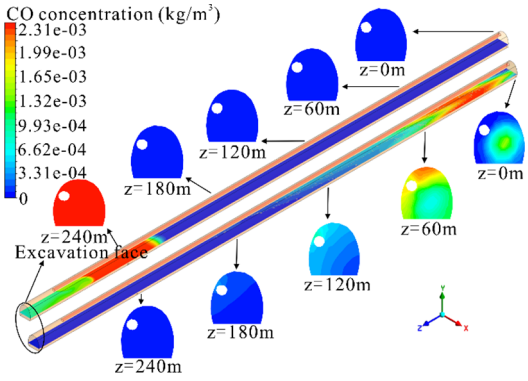

Figure 9. Distribution of CO at the position of the arch waist.

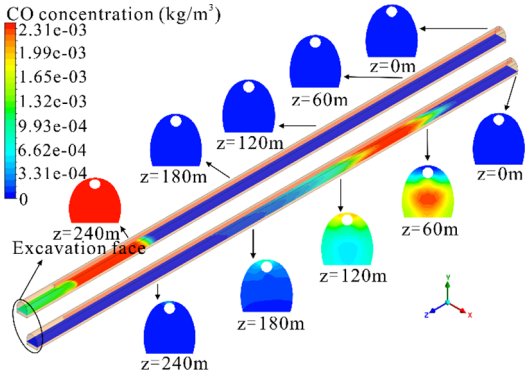

Figure 10. Distribution of CO at the location of the vault.

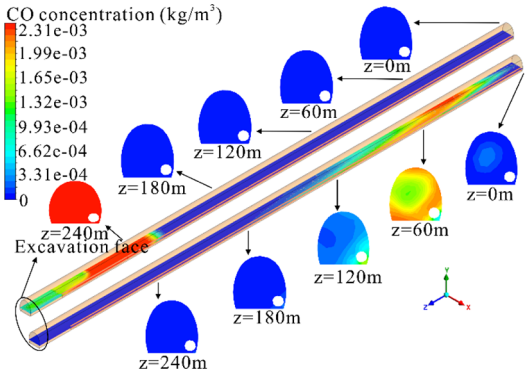

Figure 11. Distribution of CO at the position of the foot of the arch.

of arrangement when the ventilation time is 60 s. When the ducts were arranged on both sides and the ventilation time is 660 s, the CO air mass in the back of the tunnel will leave a long and thin high-concentration belt on the side of the ducts; this is due to the fact that the wind speed on the side of the ducts when the ducts are arranged on both sides is slightly smaller than that on the other side. When the duct is arranged in the tunnel vault, the fresh air flow from the mouth of the duct flows uniformly to both sides of the wall, the wind speed on both sides is smaller than the wind speed at the centerline of the tunnel, and the concentration of the CO gas mass at the front end of the tunnel is lower than that in the middle of the tunnel. However, because the wind flow contacts both sides of the wall at the same time, the wind speed was significantly smaller than the other two cases when the wind flow reaches the center and back of the tunnel and the efficiency of smoke exhaust in the tunnel was affected.

https://doi.org/10.1021/acsomega.3c05280
ACS Omega 2023, 8, 42565−42575

The distribution of the CO concentration in the cross section at different duct positions at different distances from the face of the tunnel at the time of ventilation time of 60 and 660 s is shown in Figure 12 and Figure 13, and it can be seen in Figure 12

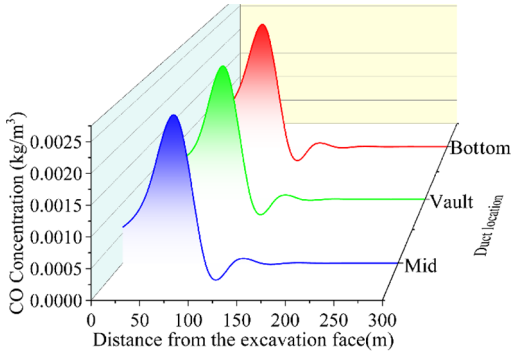

Figure 12. Variation of CO concentration at t = 60 s.

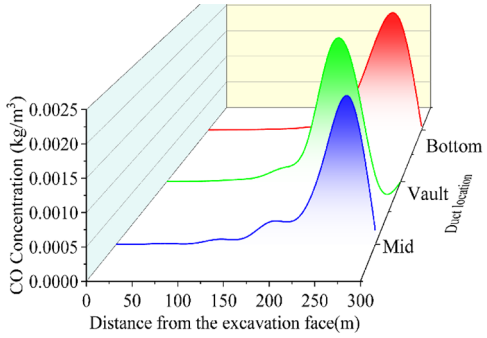

Figure 13. Variation of CO concentration at t = 660 s.

that the CO concentration in the limit distance of the throw zone, 60 m from the face of the tunnel, is the highest at the time when ventilation is first started, which is about 2450 mg/m^3. The CO distribution in the whole tunnel is low on both sides and high in the middle, and the dotted line graph shows a "convex" shape. After 660 s of ventilation, the high-concentration area was transferred to the end of the tunnel, and comparing the three point-line diagrams, we could see that the air ducts were arranged in the arch top position with the lowest smoke exhaust efficiency and the area of the high-concentration band of the point-line diagrams was smaller than that of the arch foot position when the ducts were arranged in the arch waist position, so the comprehensive comparison of the above three arrangement situations could show that the air ducts were arranged in the arch waist of the tunnel with the best smoke exhaust efficiency.

4. $MC_{(CO)}$ SPACE−TIME VARIATION MODEL

4.1. $MC_{(CO)}$ Along-Journey Variation Model. The blasting of the boring face will produce a large number of toxic and harmful gases; to a certain extent, it will pollute the tunnel construction environment, and its diffusion and transportation are more complex, difficult to control, hazardous, and easy to construction personnel's life safety and health hazards.[14] Therefore, in order to ensure the safety of the operating environment and construction personnel, CO diffusion and transport in tunnels are modeled to further project the transport and diffusion characteristics of CO gas in tunnels. In order to investigate the safety moment "15 min" specified in the *Design Specification* moment CO along the tunnel changes, according to the simulation results of the tunnel CO concentration statistics of the corresponding measurement points, CO corresponding measurement points as shown in Figure 14, the concentration of

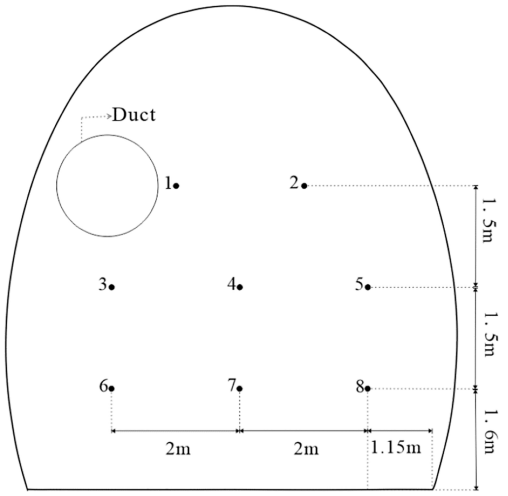

Figure 14. CO measurement point distribution.

CO at each measurement point (kg/m^3) in Table 3. Because of the large number of decimal places, it is expressed by scientific notation, and L in the table represents the distance of a vertical section from the excavation face, m.

In order to more intuitively observe the variation of CO along the course of different measurement points, the data in the table were plotted as point-line diagrams, as shown in Figure 15, and the average of the eight measurement points was fitted to finally obtain the $MC_{(CO)}$ along the course of the curve, as shown in Figure 16.

From Figure 15 and Figure 16, it could be seen that the CO concentration at measurement points 1 and 2 was higher than the other measurement points when the tunnel was ventilated for 15 min because the density of CO was slightly smaller than the density of air, which indicated that the simulation results were in line with the actual law. The concentration of CO increased with the increase of the distance from the face of the tunnel, and at this time, the concentration in the vicinity of the face of the tunnel had been lowered to 30 mg/m^3 as stipulated in the *Design Specification*, which would not be hazardous to the workers, but there was still a concentration of about 564 mg/m^3 of CO gas at the end of the tunnel, which was much larger than the safety value of 30 mg/m^3. At this point, the concentration near the tunnel face has been reduced to 30 mg/m^3 as specified in the *Design Specification*, which was not harmful to the construction workers. However, the concentration of CO gas at the tunnel tail is still about 564 mg/m^3, which is much larger than the safety value of 30 mg/m^3, indicating that continuous ventilation is still needed to completely exhaust the CO gas from the tunnel tail. In order to make the fitting curve fit the mean scattering point as much as possible, a fifth-order polynomial method is used for fitting, and it can be seen from Figure 16 that the concentration of CO is nonlinearly and positively correlated with the distance of the boring face, which can be based on the equation $y = 1.191 \times 10^{-6} - 2.612 \times 10^{-7}x + 8.397 \times 10^{-9}x^2 - 7.694 \times 10^{-11}x^3 + 2.655 \times 10^{-13}x^4 - 7.628 \times 10^{-17}x^5$.

4.2. $MC_{(CO)}$ Variation over Time Model. In order to explore the variation of CO with time in the breathing zone

https://doi.org/10.1021/acsomega.3c05280
ACS Omega 2023, 8, 42565−42575

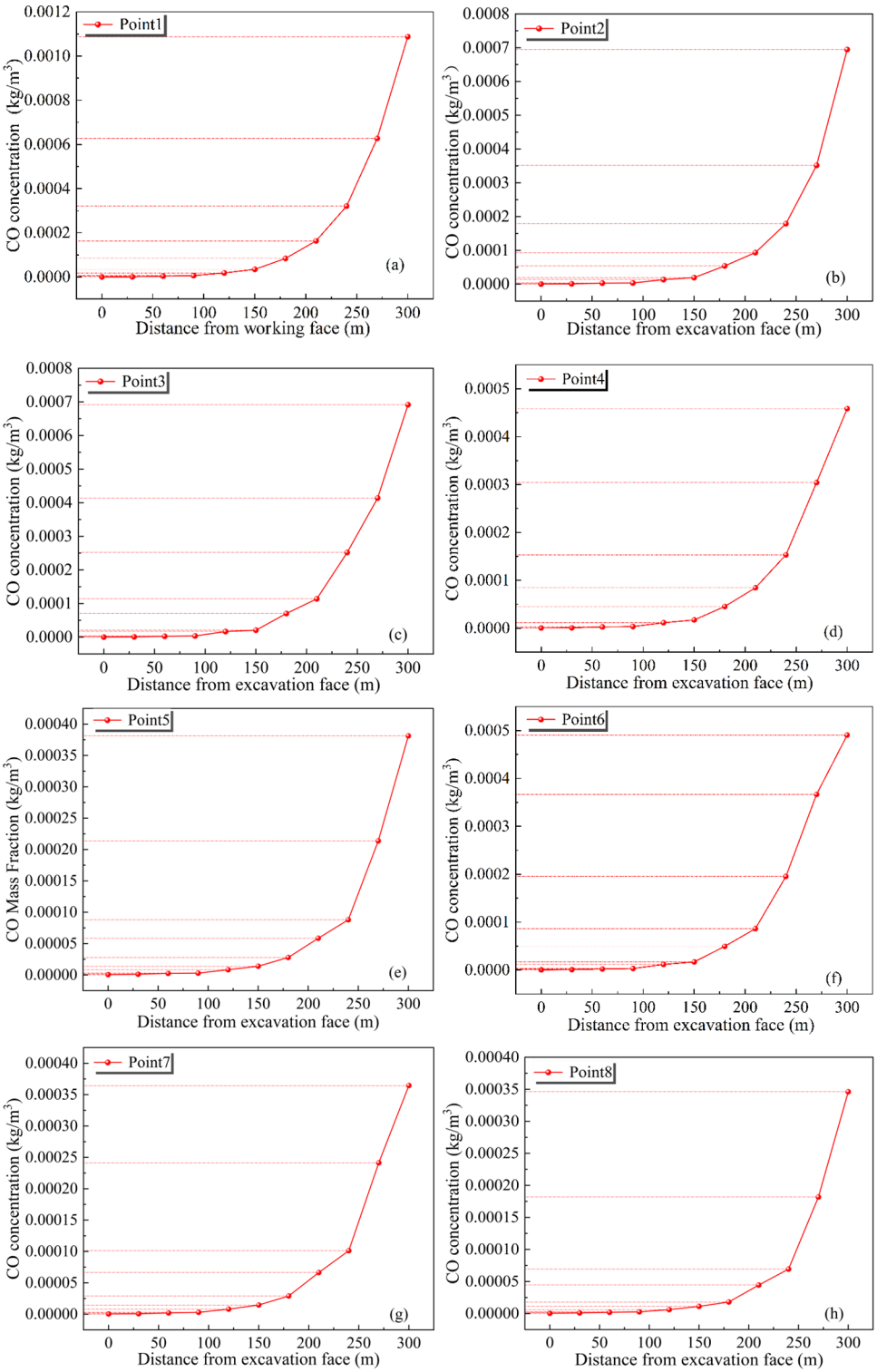

Figure 15. Variation of CO along the range of each point (a–h: the changes of the CO concentration from point 1 to point 8).

height (Y = 1.6 m) near the cross section of the air outlet of the air duct, the average value of the CO concentration of "6,7,8", three measuring points of the cross section L = 20 m, was selected for time–concentration fitting. The average concentration (kg/m^3) of the three measuring points is shown in Table 4. Considering that the maximum concentration of CO in the air outlet section at 1 and 30 min is quite different, if it is fitted as only one curve, the error will be too large. Therefore, the mixture is divided into two time periods for fitting. The fitting curves are shown in Figures 17 and 18.

As can be seen from Figures 17 and 18, the CO gas shows a nonlinear decreasing trend in the ventilation time from 1 to 30 min and the CO concentration in the cross section where the air outlet is located tends to zero when the ventilation is up to 30 min, and the air quality has been significantly improved. The CO concentration in the cross section where the air outlet is located during 1–15 min of ventilation can be calculated by the formula

https://doi.org/10.1021/acsomega.3c05280
ACS Omega 2023, 8, 42565–42575

Table 3. CO Concentration of Each Measurement Point under Different Excavation Faces

point L	1	2	3	4	5	6	7	8	Average
0	4.07×10^{-7}	5.32×10^{-7}	3.53×10^{-7}	4.36×10^{-7}	5.27×10^{-7}	3.80×10^{-7}	4.36×10^{-7}	4.91×10^{-7}	4.45×10^{-7}
60	3.82×10^{-6}	3.30×10^{-6}	2.66×10^{-6}	2.62×10^{-6}	2.44×10^{-6}	2.25×10^{-6}	2.01×10^{-6}	1.91×10^{-6}	2.62×10^{-6}
120	1.84×10^{-5}	1.35×10^{-5}	1.67×10^{-5}	1.15×10^{-5}	8.29×10^{-6}	1.17×10^{-5}	8.16×10^{-6}	6.13×10^{-6}	1.17×10^{-5}
180	8.40×10^{-5}	5.42×10^{-5}	7.04×10^{-5}	4.56×10^{-5}	2.79×10^{-5}	4.95×10^{-5}	2.91×10^{-5}	1.81×10^{-5}	4.73×10^{-5}
240	3.21×10^{-4}	1.79×10^{-4}	2.52×10^{-4}	1.53×10^{-4}	8.80×10^{-5}	1.95×10^{-4}	1.01×10^{-4}	6.94×10^{-5}	1.69×10^{-4}
300	1.09×10^{-3}	6.95×10^{-4}	6.92×10^{-4}	4.59×10^{-4}	3.81×10^{-4}	4.90×10^{-4}	3.65×10^{-4}	3.46×10^{-4}	5.64×10^{-4}

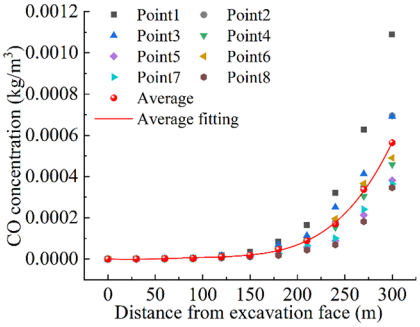

Figure 16. Variability of CO along the distance.

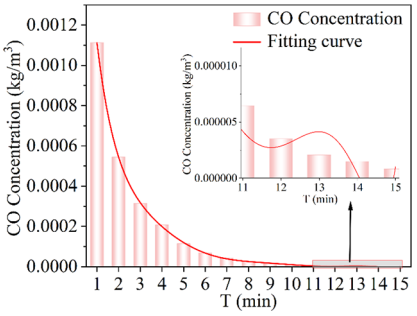

Figure 17. 1−15 min CO time−concentration fit curve.

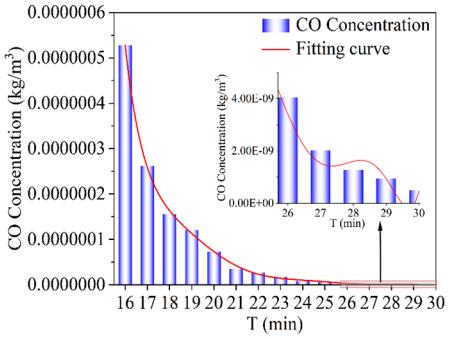

Figure 18. 16−30 min CO time−concentration fit curve.

$y = 0.00262 - 2.33 \times 10^{-3}x + 1.07 \times 10^{-3}x^2 - 2.896 \times 10^{-4}x^3 + 4.799 \times 10^{-5}x^4 - 4.894 \times 10^{-6}x^5 + 2.991 \times 10^{-7}x^6 - 1.004 \times 10^{-8}x^7 + 1.423 \times 10^{-10}x^8$. The CO concentration during 16−30 min of ventilation can be calculated by $y = 0.00691 - 0.00238x + 3.57257 \times 10^{-4}x^2 - 3.0456 \times 10 - {}^{5}x^3 + 1.6138 \times 10^{-6}x^4 - 5.4433 \times 10^{-8}x^5 + 1.4131 \times 10^{-9}x^6 - 1.3603 \times 10^{-11}x^7 + 7.0564 \times 10^{-14}x^8$.

In order to verify whether the simulation results were consistent with the on-site CO diffusion situation, the actual and simulated values of the CO concentration in different cross sections in the tunnel at the moment of 15 min, as well as the actual and simulated values of the CO concentration in the cross section of the air outlet of the wind turbine with respect to time, were selected for the comparative study. The automatic gas concentration detection device was utilized to record the CO diffusion on site, and the corresponding data comparison diagrams were drawn, as shown in Figures 19 and 20. As can be seen from Figures 19 and 20, the diffusion trend of CO in different cross sections in the tunnel is more or less the same and the measured value of its concentration is slightly higher than the simulated value. This is due to the presence of mechanical equipment at the tunnel construction site and a certain air leakage rate of the air blower, but from the overall situation, the CO diffusion pattern fluctuates less in comparison with the field situation, which is within the acceptable range. Since the effect of other altitude on CO diffusion in tunnels was not taken into account in the simulation process, the above obtained equations

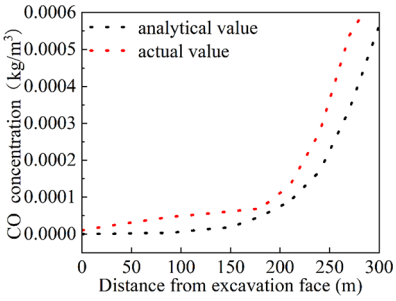

Figure 19. Comparison of simulated and measured values of the CO concentration for 15 min of ventilation.

Table 4. Average Concentration of Measurement Points near the Excavation Face

t (min)	1	2	3	4	5	6	7	8
CO concentration	1.11×10^{-3}	5.45×10^{-4}	3.14×10^{-4}	2.07×10^{-4}	1.14×10^{-4}	6.79×10^{-5}	4.21×10^{-5}	2.71×10^{-5}
t (min)	9	10	11	12	13	14	15	
CO concentration	1.55×10^{-5}	8.96×10^{-6}	6.45×10^{-6}	3.51×10^{-6}	2.06×10^{-6}	1.49×10^{-6}	8.03×10^{-7}	
t (min)	16	17	18	19	20	21	22	23
CO concentration	5.28×10^{-7}	2.62×10^{-7}	1.56×10^{-7}	1.21×10^{-7}	7.37×10^{-8}	3.48×10^{-8}	2.71×10^{-8}	1.73×10^{-8}
t (min)	24	25	26	27	28	29	30	
CO concentration	8.23×10^{-9}	5.91×10^{-9}	4.03×10^{-9}	2.01×10^{-9}	1.27×10^{-9}	9.31×10^{-10}	4.79×10^{-10}	

https://doi.org/10.1021/acsomega.3c05280
ACS Omega 2023, 8, 42565−42575

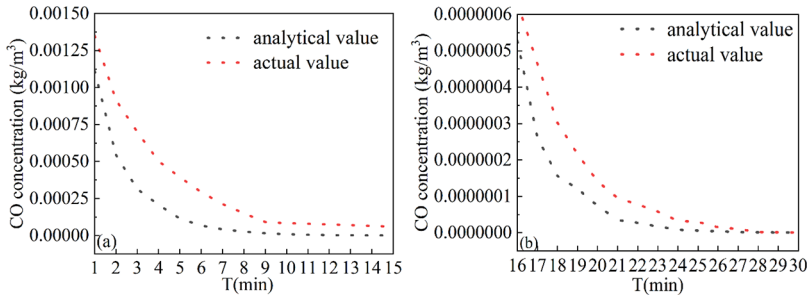

Figure 20. Comparison between the simulated value and the measured value of the CO concentration at different moments of the air outlet section (a: The changes of CO concentration from 1 to 15 min; b: The changes of CO concentration from 16 to 30 min).

are suitable for measuring CO diffusion in tunnels at an altitude of about 1500 m.

5. CONCLUSIONS

1. The wind flow in the tunnel was shot out from the pressurized wind pipe and transported along the tunnel wall, which was in line with the characteristics of the "wall-constrained jet". In the process of moving to the boring face, the wind flow diffusion section increases and the wind speed decreases gradually and the wind speed near the boring face is between 0.8 and 3.5 m/s. Under the combined effect of fresh wind and return wind, the wind flow will be reduced and the wind speed will be reduced. Under the joint action of fresh wind and returning wind, a vortex zone is formed at the front of the wind pipe mouth, and the wind speed in the vortex zone was about 0.7 m/s. The wind flow from the back of the wind pipe outlet to the exit section of the tunnel gradually tends to be stabilized.
2. In certain circumstances, the faster the air velocity at the air outlet, the higher the efficiency of smoke exhaust in the tunnel, the higher the transportation rate of harmful gases, the higher the tunnel boring surface to the air outlet area of the tunnel, and the better the improvement of harmful gases gathered. However, according to the "Design Specification", the ventilation wind speed of the whole section excavation should be between 0.15 and 6 m/s, so the wind speed cannot be increased indefinitely, the wind speed of the air outlet is 9 m/s, and the wind speed near the boring face is about 2.5 m/s to meet the requirements of the smoke exhaust;
3. The length of the smoke throwing zone was about 61 m, the CO concentration in this area peaked at about 2450 mg/m^3 in the tunnel, the exhaust efficiency was the highest in the first 15 min after the fan was turned on, and the CO mass concentration near the boring face decreased greatly during this time, but the reduction of its concentration in the subsequent time was gradually slow and the CO near the palm face of the tunnel was basically discharged when the tunnel was ventilated to 1800 s. Thus, it can be regarded as the change of the CO concentration having a "time sensitivity" to a certain extent.
4. When the duct was arranged in the waist and foot of the arch, the side wall of the duct would leave a long and thin high-concentration band because of the difference in wind speed, and the proportion of high concentration would be larger at this time. When the duct was arranged at the top of the arch, the wind speed to the two sides of the wall, respectively, will be significantly smaller than the remaining two cases; the comparative analysis of the duct was arranged in the waist of the arch when the smoke exhaust efficiency was optimal.
5. During the construction of high-altitude tunnels, there were always some differences in the CO transport pattern and concentration distribution due to the differences in ventilation time, outlet wind speed, duct arrangement, and CO transport distance. When the ventilation time was 15 min, the CO concentration in different sections of the tunnel was nonlinearly positively correlated with the distance from the boring face; when the wind speed was 9 m/s and the ventilation time was 30 min, the CO concentration in the outlet section had a nonlinearly decreasing tendency with the change of time and the CO concentration in different cases could be calculated by different $MC_{(CO)}$ models.

AUTHOR INFORMATION

Corresponding Author

Wanqing Wang − *School of Finance, Yunnan University of Finance and Economics, Kunming 650221, China;* orcid.org/0009-0002-4153-0975; Email: zz2127@ynufe.edu.cn

Authors

Jie Liu − *Faculty of Public Security and Emergency Management, Kunming University of Science and Technology, Kunming 650093, China*

Huyun Zhao − *Faculty of Public Security and Emergency Management, Kunming University of Science and Technology, Kunming 650093, China*

Haowen Zhou − *Faculty of Public Security and Emergency Management, Kunming University of Science and Technology, Kunming 650093, China*

Feng Lu − *Faculty of Public Security and Emergency Management, Kunming University of Science and Technology, Kunming 650093, China*

Liting Wan − *Faculty of Public Security and Emergency Management, Kunming University of Science and Technology, Kunming 650093, China*

Xuehua Luo − *Faculty of Public Security and Emergency Management, Kunming University of Science and Technology, Kunming 650093, China*

Liangyun Teng − *Faculty of Public Security and Emergency Management, Kunming University of Science and Technology, Kunming 650093, China*

Complete contact information is available at: https://pubs.acs.org/10.1021/acsomega.3c05280

https://doi.org/10.1021/acsomega.3c05280
ACS Omega 2023, 8, 42565−42575

Notes

The authors declare no competing financial interest.

■ ACKNOWLEDGMENTS

This research was funded by the Yunnan Province Key R&D Program Project (grant number 202003AC100002) and the Scientific Research Fund Project of Yunnan University of Finance and Economics (grant number 2021D04). Constructive comments by anonymous reviewers and the editor are highly appreciated.

■ REFERENCES

(1) Tian, S. M.; Wang, W.; Yang, C. Y.; Liu, C.; Wang, M. N.; Wang, K. J.; Ma, Z. F.; Lv, G. Development and Prospect of Railway Tunnels in China in Recent 40 Years. *Tunnel Construction* **2021**, *41* (11), 1903−1930.

(2) West, J. B. High-altitude medicine. *Am. J. Respir. Crit. Care Med.* **2012**, *186* (12), 1229−1237.

(3) Baur, X.; Sanyal, S.; Abraham, J. L. Mixed-dust pneumoconiosis: Review of diagnostic and classification problems with presentation of a work-related case. *Sci. Total Environ.* **2019**, *652*, 413.

(4) Ulvestad, B.; Bakke, B.; Melbostad, E.; Fuglerud, P.; Kongerud, J.; Lund, M. B. Increased risk of obstructive pulmonary disease in tunnel workers. *Thorax* **2000**, *55* (4), 277.

(5) Whayne, T. F., Jr. Cardiovascular medicine at high altitude. *Angiology* **2014**, *65* (6), 459−472.

(6) Menéndez, J.; Merlé, N.; Fernández-Oro, J. M.; Galdo, M.; de Prado, L. Á.; Loredo, J.; Bernardo-Sánchez, A. Concentration, Propagation and Dilution of Toxic Gases in Underground Excavations under Different Ventilation Modes. *Int. J. Environ. Res. Public Health* **2022**, *19* (12), 7092.

(7) Liu, Q.; Cheng, W.; Liu, L.; Hua, Y.; Guo, L.; Nie, W. Research on the control law of dust in the main ventilation system in excavated tunnels for cleaner production. *Build. Environ.* **2021**, *205*, No. 108282.

(8) Harris, M. L.; Mainiero, R. J. Monitoring and removal of CO in blasting operations. *Saf. Sci.* **2007**, *46* (10), 1393−1405.

(9) Wu, B; Zhao, R; Meng, G; Xu, S; Qiu, W; Chen, H A numerical study on CO migration after blasting in high-altitude tunnel by inclined shaft. *Sci. Rep.* **2022**, *12* (1), 14696.

(10) Huang, R.; Shen, X.; Wang, B.; Liao, X. Migration characteristics of CO under forced ventilation after excavation roadway blasting: A case study in a plateau mine. *J. Cleaner Prod.* **2020**, *267*, No. 122094.

(11) Pu, Q.; Luo, Y.; Huang, J.; Zhu, Y.; Hu, S.; Pei, C.; Zhang, G.; Li, X.; Rafiee, M. Simulation Study on the Effect of Forced Ventilation in Tunnel under Single-Head Drilling and Blasting. *Shock Vib.* **2020**, *2020*, 1.

(12) Klanfar, M.; Vrkljan, D.; Lončarić, M. Kvaliteta zraka i mikroklimatski parametri pri iskopu tunela Mala Kapela/Air Quality and Microclimatic Parameters During Excavation of Mala Kapela Tunnel. *Rudarsko - Geolosko - Naftni Zbornik* **2015**, *30* (1), 55.

(13) Torno, S.; Torano, J.; Ulecia, M.; et al. Conventional and numerical models of blasting gas behaviour in auxiliary ventilation of mining headings[J]. *Tunnelling & Underground Space Technology* **2013**, *34* (34), 73−81.

(14) Liu, J.; Zhou, H.; Wang, W.; Hu, X.; Ma, Q.; Lu, F. Study of the Diffusion Law of Harmful Gases in Tunnel Construction on Plateaus and Optimization of Ventilation Parameters. *ACS Omega* **2022**, *7* (31), 27135.

(15) Wen, H; Mi, W; Fan, S; Xu, Y; Cheng, X Simulation study on crucial parameters of long-compressive and short-suction ventilation in large section roadway excavation of LongWangGou coal mine. *Environ. Sci. Pollut. Res. Int.* **2022**, *30*, 6435.

(16) Hua, Y.; Nie, W.; Liu, Q.; Liu, X.; Liu, C.; Zhou, W.; Yu, F. Analysis of diffusion behavior of harmful emissions from trackless rubber-wheel diesel vehicles in underground coal mines. *Int. J. Min. Sci. Technol.* **2022**, *32* (6), 1285.

(17) Voronstov, A. G. Monitoring system for the operation of the main ventilation system. *Fuel Energy Abstr.* **1997**, *4* (38), 267.

(18) Fang, Y.; Yao, Z.; Lei, S. Air flow and gas dispersion in the forced ventilation of a road tunnel during construction. *Underground Space* **2019**, *4* (2), 168.

(19) Li, Z.; Lin, X.; Li, M.; Zhang, W.; Rao, B. Simulation analysis of CO diffusion for double tube tunneling excavated from single end. *J. Railway Sci. Eng.* **2013**, *10* (04), 82−87.

(20) Zhou, X.-Q.; Wu, B.; Du, H. B. Theoretical Study on Fundamental Conceptions in Mine Ventilation Theory. *J. Chin. Univ. Min. Technol.* **2003**, *32*, 133−137.

(21) Junxin, H. A Study on Optimization of Control Algorithm and Key Technologies of 3D Visualization for Mine Ventilation System. Central South University, 2012.

(22) Lu, X. M.; Yin, H. The intelligent theory and technology of mine ventilation. *J. Chin. Coal Soc.* **2020**, *45* (06), 2236−2247.

(23) Shao, L.; Zhen, W.; Li, C. Optimization Algorithm of Mine Ventilation Based on SA-IPSO. *J. Syst. Simul.* **2021**, *33* (09), 2085−2094.

(24) Jiang, Z.; Li, T.; Zhang, Z. Numerical Simulation of the Airlow Field Rules in Tunnel Drill Blasting Construction. *Ind. Saf. Environ. Prot.* **2016**, *42* (08), 53−55 + 60.

(25) Jushi, C.; Yi, W.; Zhongan, J. Numerical simulation of blasting dust concentration distribution and diffusion regularities in stope. *J. China Coal Soc.* **2013**, *38* (S1), 147−152.

(26) Fan, L.; Chuan, Y.; Jianzhong, C.; Shiqiang, D.; Shuai, L. Numerical simulation of the effect of the angle of merging section on ventilation characteristics in highway tunnels. *Mod. Tunnelling Technol.* **2020**, *57* (S1), 645−650.

(27) Wang, Y. D.; Xia, X. Y. Numerical simulation of longitudinal ventilation of highway tunnel. *China J. Highw. Transp.* **2002**, *01*, 85−88.

(28) Lijun, S.; Wenbo, L. Study on Diffusion of Blasting Fumes and Ventilation Technique during Construction of Underground Tunnel. *Blasting* **2000**, *01*, 1−6.

(29) Gao, W.-J.; Liang, J.-Q.; Xu, J.-J.; Xia, F.-S. Discussion on the Blasting and Driving Ventilation of Dead-End Drift. *Min. Metall. Eng.* **2021**, *41* (03), 16−20.

(30) Wu, B.; Chen, H.-H.; Huang, W. W. Analysis of Forced Ventilation Flow Field in Railway Tunnel and Optimization of Construction Parameters. *Sci. Technol. Eng.* **2021**, *21* (07), 2922−2928.

(31) Chen, L. Application of Gallery Ventilation Technology and Energy Conservation Heating Technology to Guanjiao Tunnel. *Tunnel Construction* **2016**, *36* (07), 857−861.

(32) Ding, C.; Nie, B.; Sun, D. Study on the natural diffusion model of blasting smoke in tunnel construction. *Min. Saf. Environ. Prot.* **2022**, *49* (04), 117−122.

(33) Ye, Y.-J.; Jiang, J.-T.; Ding, D.-X.; Zhong, Y.-M.; Xie, C. Transport of radon and blasting-fume in blind roadway with exhaust ventilation after blasting. *China Saf. Sci. J.* **2015**, *25* (05), 131−137.

(34) Ji, H. G.; Cao, Y.; Zhang, G; Li, S.; Chen, B.; Jiang, H. Prediction of Drain-fume Time of Single-end Roadway in Tunneling Process. *Met. Mine* **2014**, *05*, 142−145.

(35) Yanhua, Zeng; Kangfu, Peng Research on the Construction Ventilation Technique for the Spiral Ramp Laneway in High-elevation Mine [J]. *Metal Mine* **2018**, No. 11, 126−132.

(36) Juganda, A.; Strebinger, C.; Brune, J. F.; et al. Discrete modeling of a longwall coal mine gob for CFD simulation[J]. International Journal of. *Mining Science and Technology* **2020**, *30* (4), 463−469.

(37) Brodny, J.; Tutak, M. Applying computational fluid dynamics in research on ventilation safety during underground hard coal mining: A systematic literature review[J]. *Process Safety and Environmental Protection* **2021**, *151*, 373−400.

(38) Zhang, G.; Jaing, S.; Wang, R. Analysis of CO Distribution and Air Demand during Slagging in High Altitude Tunnel. *J. Hunan Univ. (Nat. Sci.)* **2021**, *48* (12), 174−184.

(39) Cao, Z.; Yang, Q.; Guo, C. Migration characteristics of poisonous gas during construction stage in railway tunnels at high altitude areas. *J. Cent. South Univ. (Sci. Technol.)* **2016**, *47* (11), 3948−3957.

https://doi.org/10.1021/acsomega.3c05280
ACS Omega 2023, 8, 42565−42575